OXFORD

BIOLOGY Methods & Protocols

Biology Methods and Protocols, 2025, **10(1)**, bpaf030

https://doi.org/10.1093/biomethods/bpaf030
Advance Access Publication Date: 11 April 2025
Methods Article

A deep learning pipeline for morphological and viability assessment of 3D cancer cell spheroids

Ajay K. Mali[1], Sivasubramanian Murugappan[1], Jayashree Rajesh Prasad[2], Syed A. M. Tofail[1,3] and Nanasaheb D. Thorat[1,3,*]

[1]Department of Physics and Bernal Institute, University of Limerick, Castletroy, Limerick, V94T9PX, Ireland
[2]Computer Science and Engineering, School of Computing, MIT Art Design and Technology University, Pune, Maharashtra, 412201, India
[3]Limerick Digital Cancer Research Centre (LDCRC), University of Limerick, Castletroy, Limerick, V94T9PX, Ireland

*Corresponding author. Department of Physics, University of Limerick, Castletroy, Limerick V94T9PX, Ireland. Email: nanasaheb.d.thorat@ul.ie

Abstract

Three-dimensional (3D) spheroid models have advanced cancer research by better mimicking the tumour microenvironment compared to traditional **two**-dimensional cell cultures. However, challenges persist in high-throughput analysis of morphological characteristics and cell viability, as traditional methods like manual fluorescence analysis are labour-intensive and inconsistent. Existing AI-based approaches often address segmentation or classification in isolation, lacking an integrated workflow. We propose a scalable, two-stage deep learning pipeline to address these gaps: (i) a U-Net model for precise detection and segmentation of 3D spheroids from microscopic images, achieving 95% prediction accuracy, and (ii) a CNN Regression Hybrid method for estimating live/dead cell percentages and classifying spheroids, with an R^2value of 98%. This end-to-end pipeline automates cell viability quantification and generates key morphological parameters for spheroid growth kinetics. By integrating segmentation and analysis, our method addresses environmental variability and morphological characterization challenges, offering a robust tool for drug discovery, toxicity screening, and clinical research. This approach significantly improves efficiency and scalability of 3D spheroid evaluations, paving the way for advancements in cancer therapeutics.

Keywords: artificial intelligence; convolutional neural network; drug discovery; high-throughput screening; live/dead assay; spheroid viability, toxicology, U-Net

Introduction

Three-dimensional (3D) spheroid models have revolutionized cancer research by better mimicking the tumour microenvironment compared to traditional two-dimensional cultures [1, 2]. These models provide crucial insights into tumour growth kinetics, drug responses, and cellular interactions. However, the complex structure of 3D spheroids and the challenges of fluorescence imaging present significant barriers to automated, high-throughput analysis [3, 4].

Deep learning has emerged as a powerful tool for biological image analysis, offering exceptional performance in segmentation, classification, and quantitative evaluation tasks [4, 5]. Among these, U-Net, a deep learning architecture tailored for biomedical image segmentation, has proven highly effective in extracting regions of interest (ROIs) such as spheroids and nuclei from fluorescence images [6, 7]. U-Net was developed by Ronneberger *et al.* [8] as an effective tool for the segmentation of cellular structures. Its ability to capture fine details and contextual features makes it particularly suitable for 3D spheroid segmentation in fluorescence microscopy [7, 9]. Complementing U-Net, convolutional neural networks (CNNs) have demonstrated robust predictive capabilities, especially when coupled with regression layers for continuous variable estimation, such as live/dead cell percentages in live/dead assays [10, 11, 12].

Despite these advances, current approaches often address segmentation or viability analysis in isolation. For instance, the study titled 'SpheroidJ: An open-source tools for spheroid segmentation' [13] introduces tools specifically designed for spheroid segmentation but did not assess viability. Conversely, 'Deep Learning unlocks Label-Free Viability Assessment of Cancer Spheroids' [14] proposed a deep learning model for viability assessment without incorporating segmentation limiting their utility in high-throughput workflows. Traditional threshold-based fluorescence quantification methods remain prone to variability from imaging conditions and user bias [15, 16]. To address these gaps, we propose a two-stage deep learning pipeline that integrates U-Net for precise spheroid segmentation and a CNN Regression model for cell viability prediction. This approach facilitates comprehensive fluorescence image analysis, automates morphological characterization, and ensures scalability for applications like drug discovery and toxicity screening.

Our pipeline addresses critical challenges in spheroid analysis, including variability in growth dynamics, imaging inconsistencies, and the need for reproducible high-throughput evaluations. By integrating segmentation and viability assessment into a unified framework, the proposed method offers a robust, scalable, and automated solution for advancing cancer research [7, 17].

Received: 17 March 2025; **Revised:** 2 April 2025; **Editorial decision:** 4 April 2025; **Accepted:** 9 April 2025

Materials and methods

Spheroid preparation and live/dead assay

3D spheroids were prepared using glioblastoma (U87) and neuroblastoma (SH-SY5Y) cell lines to model tumour heterogeneity. A co-culture method, adapted from prior research, mimicked the tumour microenvironment. Live/dead assays were performed using fluorescein diacetate (FDA) (green fluorescence for live cells) and propidium Iodide (PI) (red fluorescence for dead cells). Samples were incubated for 15 minutes at 37°C before excess dye was removed [18]. This combination provides a robust in vitro model to replicate glioblastoma's complex cellular interactions.

The live/dead assay was used to evaluate the spheroid's cell viability. Viable cells were separated from those with affected cells using FDA, which emits green fluorescence to identify live cells, and PI, which emits red fluorescence to show dead cells. The used method ensures enhanced precision in assessing the viability of cells within the spheroid [18].

The MCF-7 cells were gifted by Dr Amira Mahdi (University of Limerick). The cells were cultured in a DMEM media supplemented with 10% foetal bovine serum (Cytiva Hy Clone), 1% penicillin-streptomycin, and 1% L-glutamine (Merck Life Sciences). The trypsin and phosphate buffer saline (PBS) (Merck Life Sciences) were used for washing and detachment of cells; both were also obtained from Merck life sciences. The cells were maintained in 37°C and 5% CO_2. Flat-bottomed 96-well plates were coated with 1% agarose solution. Then, cell suspensions with cell densities of 4000, 6000, and 8000 per well were cultured. The spheroids were grown for 14 days. On the 4th- , 7th-, and 10th days, media were changed after imaging. Phase contrast microscope images of the spheroids were taken each day using a Keyence BZ-X810 Microscope.

Image acquisition and preprocessing

Fluorescence images were captured using a confocal microscope and resized to 128 × 128 pixels to reduce computational complexity while preserving morphological features. Standardization of image dimensions minimized variability and facilitated consistent training for the deep learning models [19, 20]. To enhance the model's generalizability, the training images were acquired from several independent spheroid batches under slightly varied imaging conditions (e.g., different passages, days and imaging sessions). We also applied data augmentation including random rotations, flips, and brightness/contrast to expand the diversity of imaging scenarios encountered during training. This strategy of augmenting microscopy data is known to improve a model's robustness to variations in imaging setup [21], helping the model maintain performance even if the new images have different illumination or background characteristics. By lowering image size, researchers may regulate the additional storage space and processing time necessary for larger images, allowing for more effective analysis in limited in resources situations [22].

Spheroid segmentation using U-Net

The U-Net model was employed for spheroid segmentation. Training used 500 annotated fluorescence images, with segmentation masks created in ImageJ. Key hyper parameters included a learning rate of 0.001, 20 epochs, and binary cross-entropy loss. Data augmentation (rotation, flipping, intensity scaling) enhanced generalization [23, 24, 25]. Post-segmentation, morphological filtering was applied to isolate ROIs [12].The workflow for the U-Net model is shown in **Fig. 1**.

Cross-validation technique

To improve model performance and prevent overfitting, K-fold cross-validation (K = 10) was implemented. This involved dividing the dataset into 10 separate folds, iteratively training on nine folds and validating on the remaining fold, so providing an accurate evaluation of model generalization across various data subsets [27]. The accuracy of predictions was assessed using measures like the coefficient of determination, R^2, and mean absolute error (MAE). The model demonstrated significant predictive performance by achieving a high R^2 value of 97% on the test datasets. The model's performance consistency and predictability are further demonstrated by the MAE graph across folds and the accuracy and loss graphs for each fold (see Supplementary Figs. 1, 2, and 3).

Viability prediction using CNN + regression

The segmented ROIs were input to a CNN-based regression model to predict live and dead cell percentages. The CNN architecture included convolutional layers with ReLU activation, max-pooling, and a regression output layer. Ground truth viability data were derived from fluorescence intensity ratios of PI and FDA channels. A 10-fold cross-validation method was used to split the dataset into training and testing subsets, providing an extraordinary predictive accuracy with a mean R^2 value of across

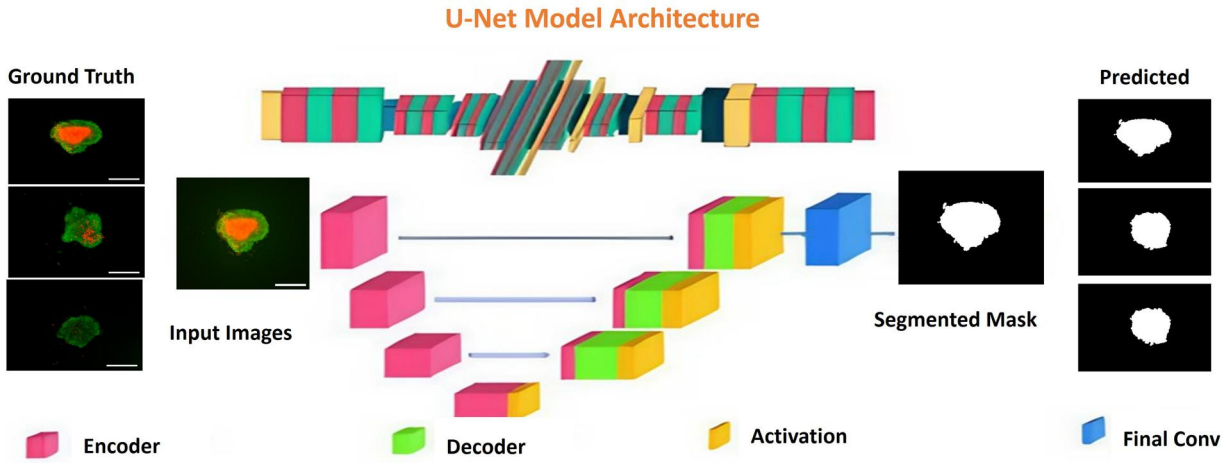

Figure 1. U-Net model procedure. It starts with an input image, then the encoder path (down sampling), bottleneck, and decoder path (up sampling), which includes skip connections to retain spatial information for accurate segmentation (U-Net model architecture in Fig. 1 modified from [26]

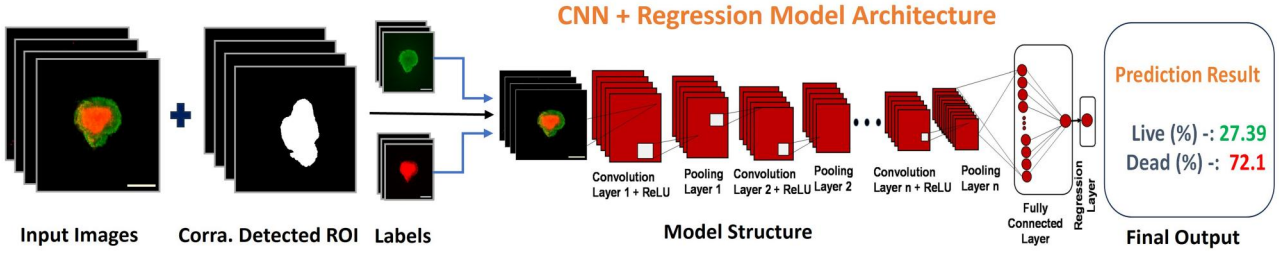

Figure 2. The CNN + Regression model procedure. The CNN collects relevant spatial information from the input image and passes them to a regression layer, which predicts continuous output of live and dead cell percentages (Model structure in Fig. 2 modified from [28]

all folds are 89%. The workflow for the CNN Regression Hybrid model is demonstrated in **Fig. 2**.

Morphological analysis

Morphological metrics, such as spheroid area, sphericity, and roundness, were measured using Python libraries (scikit-image, OpenCV) and ImageJ [29]. Results were cross-validated, showing Python-based methods to be more efficient and consistent [30, 31].

Evaluation matrices

For segmentation, dice similarity coefficient (DSC) and Intersection Over Union (IoU) quantified overlap between predicted and ground truth masks. For viability prediction, R^2 and MAE assessed model performance. These metrics ensured balanced evaluation across imbalanced datasets and provided insights into prediction accuracy.

For spheroid segmentation (U-Net model)

DSC

The U-Net model's performance was assessed using the DSC to quantify the overlap between the predicted segmentation (P) and the ground truth (G) masks. The DSC is defined is as Eq. (1):

$$\mathrm{DSC} = \frac{2 \times |P \cap G|}{|P| + |G|} \tag{1}$$

The dice coefficient is extensively utilized in medical image analysis due to its ability to demonstrate consistency in overlapping regions, making it particularly successful for segmentation tasks. This is particularly crucial for situations such as spheroid segmentation, when precision in border identification is critical. Unlike pixel accuracy, DSC penalizes both false positive and false negatives, ensuring a balanced evaluation for highly imbalanced datasets typical in medical imaging [32, 33].

IoU

It is another overlap-based metric, which measures the ratio of the intersection to the union of the predicted and ground truth masks. The IoU defined as Eq. (2):

$$\mathrm{IoU} = \frac{|P \cap G|}{|P \cup G|} \tag{2}$$

IoU enhances the DSC by providing a more comprehensive assessment, particularly sensitive to the presence of false positives. It is often used in medical image analysis because it can constantly evaluate both small and large frameworks, making sure that segmentation works well across a range of spheroidal sizes and imaging conditions [32, 33].

For live/dead viability prediction (CNN regression model)

Coefficient of determination (R^2)

The R^2metric, or the coefficient of determination, assesses how well the predicted values ($\hat{y}$)approximate the actual value (y). It is mathematically expressed as Eq. (3):

$$R^2 = 1 - \frac{\sum (y - \hat{y})^2}{\sum (y - \bar{y})^2} \tag{3}$$

- $\bar{y}$: Mean of actual values.
- An R^2 close to 1 reflects excellent predictive performance captures the ratio of variability explained by the model, giving insights into its predicative power [34].

MAE

MAE measures the average absolute differences between predicted and actual values. The MAE values defined as Eq. (4):

$$\mathrm{MAE} = \frac{1}{n}\sum_{i=1}^{n} |y_i - \hat{y}_i| \tag{4}$$

where

- y_i = actual values
- $\hat{y}_i$ = predicted values
- n = number of data points

MAE is widely used in regression tasks to assess model performance by quantifying the magnitude of errors. For live/dead prediction, MAE provides a simple interpretation of average prediction errors, allowing researchers to identify practical limitations in viability quantification [35].

Computational setup

Models were developed using Python libraries (TensorFlow, Keras, scikit-image) and trained on an NVIDIA RTX 3090 GPU. The computational pipeline was optimized for resource efficiency without compromising accuracy.

Results

U-Net spheroid detection and segmentation accuracy

In this segment, we demonstrate the efficacy of the U-Net model for spheroid detection and segmentation. To evaluate precision, the model's segmentation outputs were juxtaposed with manually annotated ground truth masks. The U-Net model excels at segmenting spheroids characterized by clear boundaries and

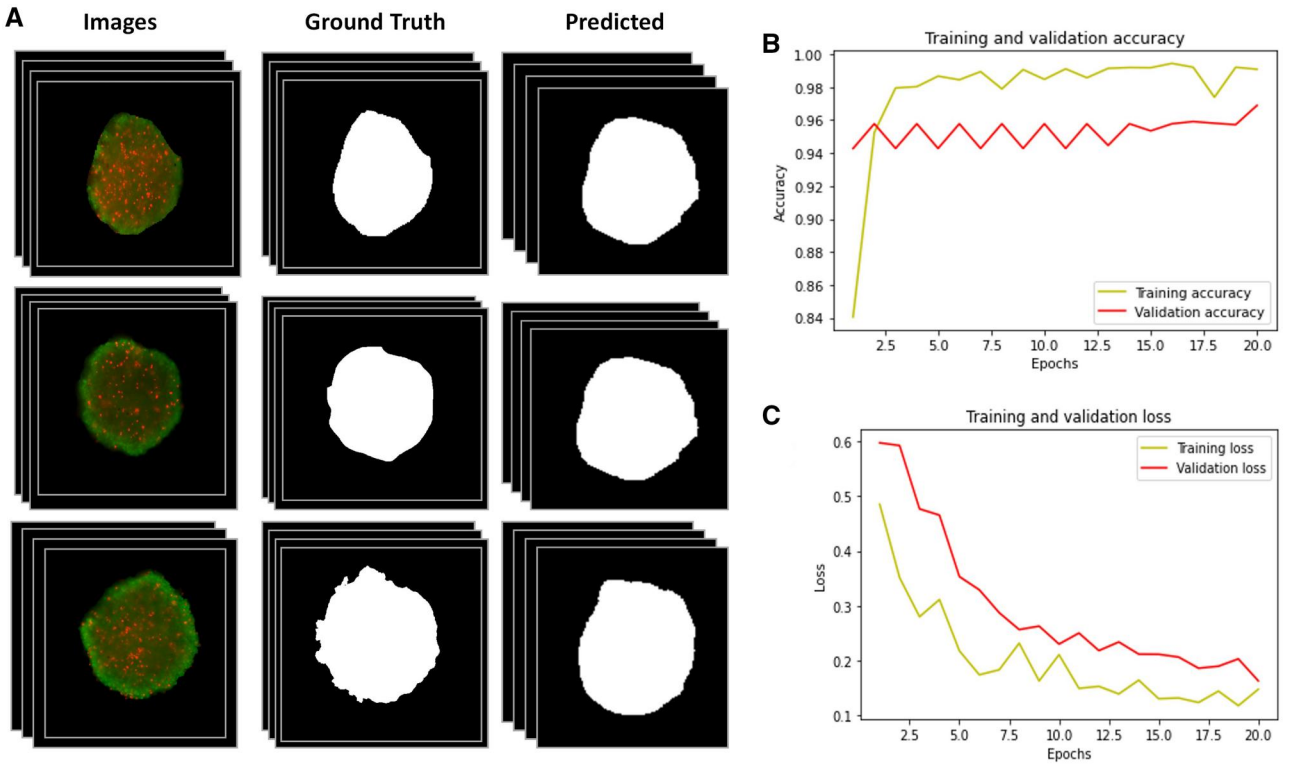

Figure 3. Results of spheroid segmentation using the U-Net model. A) The left column shows the original fluorescence images, followed by the corresponding ground truth masks (manually annotated using ImageJ) and the predicted segmentation masks by the model. The quantitative assessment revealed a dice coefficient of 95%, signifying considerable overlap between the expected and actual masks. The training and validation performance curves demonstrate the model's efficacy in learning and generalizing spheroid segmentation. The training accuracy steadily improved to a peak of 98%, while validation accuracy consistently above 96%, demonstrating the model's high precision across datasets. The loss curves demonstrate consistent advancement, with training loss decreasing to roughly 0.05 and validation loss stabilizing at around 0.1 after 20 epochs. This indicates negligible overfitting and validates the model's strong ability to segment spheroids with high reliability. The persistent disparity between training and validation loss indicates the model's capacity to generalize proficiently to unfamiliar data

uniform fluorescence intensity, achieving high accuracy even in images with minimal background noise or distinctly defined spheroids (**Fig. 3**). However, complexity occurs in images with overlapping spheroids or significant background objects, leading the model to sometimes misclassify areas or insufficiently define boundaries. These occurrences underscored the necessity for sophisticated preprocessing methods or supplementary training data to enhance segmentation precision in these complex scenarios. Despite those challenges, the model's general robustness was apparent from its constant dice coefficient of 95% and precision of 98% (Supplementary Fig. 4) in detecting spheroid regions from the background. Segmentation accuracy was evaluated using metrics including the dice coefficient, IoU, and pixel-wise accuracy (Supplementary Fig. 4), demonstrating the model's proficiency in reliably segmenting spheroids across diverse image datasets. The segmentation masks generated by the U-Net model closely matched the ground truth, confirming the model's robustness and reliability.

Viability prediction outcomes

The CNN-based regression model quantified the proportions of live and dead cells in the segmented spheroid, with predictions validated by manual cell counts derived from fluorescence intensity ratios PI (live cells) and FDA (dead cells). The results, illustrated in the 'Accuracy of Live Percentage Prediction' and 'Accuracy of Dead Percentage Prediction' graphs, exhibit a strong correlation between the actual and predicted values for both live and dead cell percentages (**Fig. 4**). In Image-3, the predicted live proportion (94.8%) closely matches the actual live percentage (100%), while the expected dead percentage (4.53%) aligns with the very negligible actual dead percentage, highlighting the model's precision in extreme scenarios.

Across other images, the model performs consistently with low mistakes. Notably, the error bars in the graphs indicate confidence interval, which helps to validate the forecasts' robustness. The R^2 score of 0.98 indicates a great fit between predicted and actual values, capturing 98% of the variability in the data.

The second graph, 'R^2 per Fold', illustrates the model's stability and generalizability during cross-validation. The R^2 values consistently remain elevated across 10 folds, varying from 0.91 to 0.98. The initial fold (Fold-1) is markedly lower at 0.31. The variance in the initial fold is possibly due to data partitioning, potentially implemented in challenging scenarios during that fold. The overall trend of R^2 values indicates a well-trained and dependable model that can generalize new data.

The model has good predictive accuracy; however, there are slight gaps, such as a ± 4% error in live percentage forecasts in Image-2 and a lower R^2 value of 0.31 in Fold-1 during cross-validation, which may be attributed to dataset splitting. These constraints indicate areas for improvement, such as increasing the dataset or improving resilience with additional regularization techniques.

These findings highlight the model's capability to automate live-dead cell classification tasks with high precision, notably reducing the necessity for manual involvement. This automation can enhance throughput in high-content drug screening and

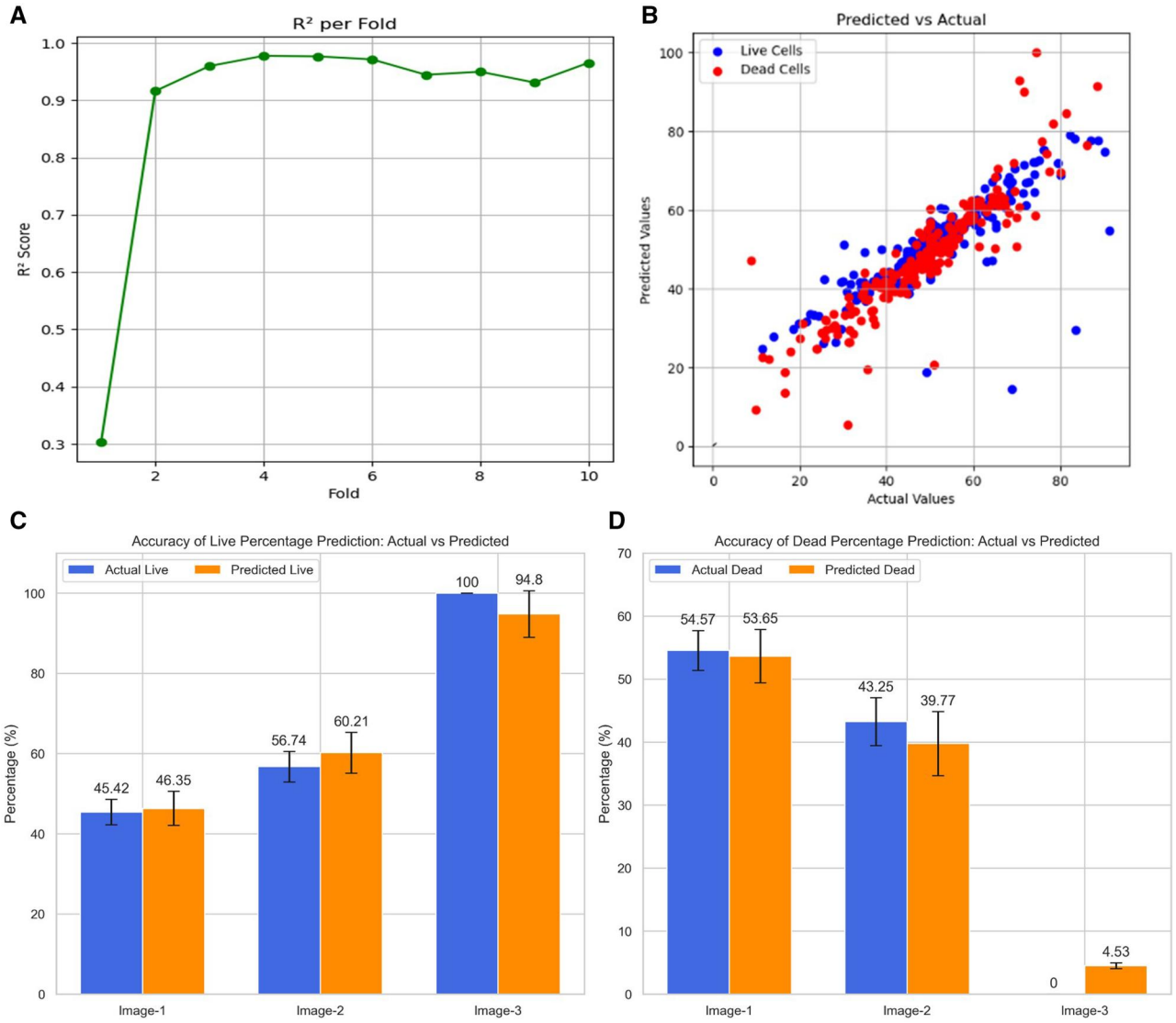

Figure 4. A) **R^2 per fold across 10-fold cross-validation**: The R2 values obtained during cross-validation are displayed in the plot. Except for a marginally lower result in Fold-1, the model consistently obtains excellent R^2 scores (0.91–0.98) across all folds. This shows how well the model predicts viability percentages with the least amount of error, demonstrating its generalizability and robustness. B) **The scatter plot of actual vs. predicted percentages** shows a close alignment of data points along the diagonal line, indicating a significant positive correlation between the two. This demonstrates how well the model predicts the percentages of live and dead cells under various experimental settings. C) **Accuracy of live percentage prediction** and D) **Dead percentage prediction**: The bar charts illustrate the actual and predicted percentages of viable and non-viable cells for three spheroid images, with error bars denoting the associated errors. The CNN-based regression model has significant accuracy in aligning predictions with manual counts. Image-3 distinctly demonstrates the model's capacity to accurately forecast extreme scenarios (e.g., 100% live and 4.53% dead)

enable accurate viability evaluation under different experimental conditions, opening the path for its implementation in both preclinical and clinical research settings.

Morphological analysis findings

The morphological analysis concentrated on the spheroid's growth kinetics, how culturing density affected spheroid development, and how morphological metrics changed over time. Both automatic Python-based techniques and manual ImageJ analysis were used to quantify spheroid area, sphericity, and roundness. The findings showed that the spheroid grew larger over time and that the initial culturing density had a significant impact on the growth rate. Increased spheroid volume and quicker aggregation were the results of higher seeding densities (Fig. 5). While the ImageJ-based method had somewhat higher variability because of manual intervention, the Python-based approach using OpenCV and scikit-image produced more consistent and efficient measurements, according to a comparison of manual and AI-based methods.

The plots highlight the impact of initial culturing density on spheroid size by comparing the growth of MCF-7 spheroid over a period of 14 days. Three different seeding densities (4000, 6000, and 8000 cells) were evaluated, and their growth kinetics were monitored by measuring spheroid area.

Application in drug development and toxicology

To demonstrate the AI-based system's potential in drug development and toxicity testing, we ran case studies with simulated drugs. Spheroids were treated to Temoside (TMZ), a formulation of FDA-approved brain cancer active pharmaceutical ingredient

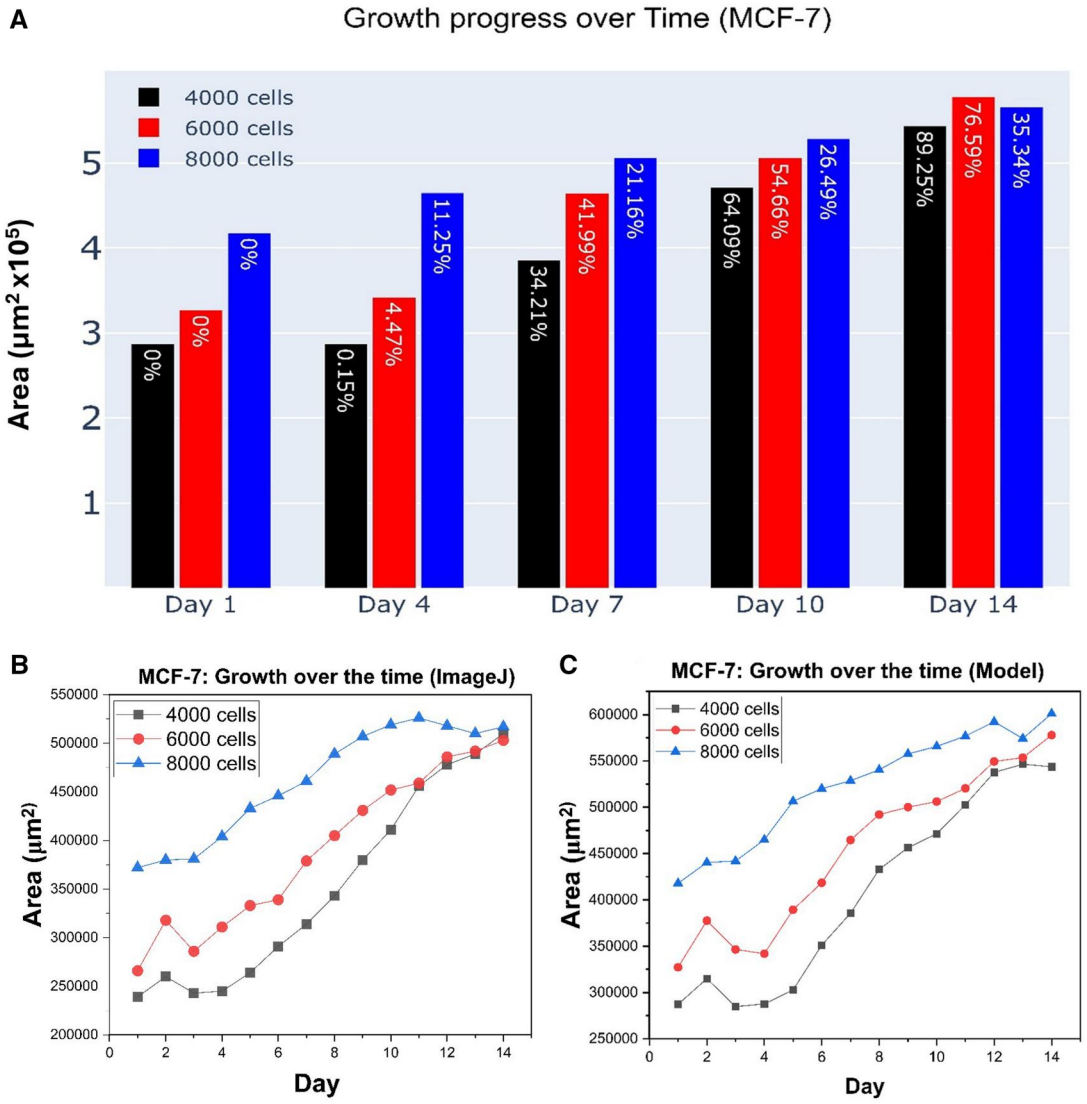

Figure 5. A) **Growth kinetics of MCF-7 spheroid**. The graphs show the spheroid growth in terms of area (in $\mu m^2 \times 10^6$) over 14 days for three different seeding densities (4000, 6000, and 8000 cells). B) This graph shows the area of the spheroid over 14 days, calculated using manual tool ImageJ. C) The graph shows the spheroid's area over a period of 14 days, as determined by our model technique. Significant parallels between the two graphs become noticeable when we look more closely

temozolomide at different concentrations (10 µM, 100 µM, and 1000 µM), and viability changes were observed. The AI system enables high-throughput screening by immediately predicting cell viability and quantifying drug treatment responses. The model was also useful in identifying dangerous chemicals, as it recognized significant cell decreases at lower drug doses, providing information on potential cytotoxic effects. These findings demonstrated how the AI system may speed up the drug discovery process, increasing efficiency and accuracy in detecting prospective drug candidates and toxicological potential dangers. When we compare these artificial intelligence (AI)-enhanced results with Manual results, it is showing notably similar results to that.

The live/dead assay visualized in **Fig. 6A** illustrates the impact of different concentrations of a TMZ drug on cellular viability of Neuroblastoma (SH-SY5Y) brain cancer cells. Images indicate that at lower drug concentrations (10 µM and 100 µM), live cells are still common throughout treatment groups, demonstrating good cell viability. Green fluorescence indicates a healthy number of live cells in the control group, while red-stained dead cells are minimal. However, at the highest dose (1000 µM), red fluorescence increases significantly, which is indicating increased cell death.

Figure 6 B presents quantitative analysis of live/dead assay visuals. Results show that cell viability in U87MG and co-cultured cells remains almost 100% at doses of 10 µM and 100 µM. Viability considerably decreases at 1000 µM, especially in the SH-SY5Y cell line, compared to other groups. The dose-dependent cytotoxic effect of TMZ shows that different cell lines respond differently to treatment.

Discussion

The application of AI-based systems for 3D spheroid analysis lines up with standards set in the field of biomedical research. Research has demonstrated that high-throughput screening enhanced by AI can markedly decrease the duration needed to identify lead compounds for drug discovery. 3D spheroid models replicate in vivo-like circumstances and can now be analysed more efficiently and effectively using AI algorithms [36,37].

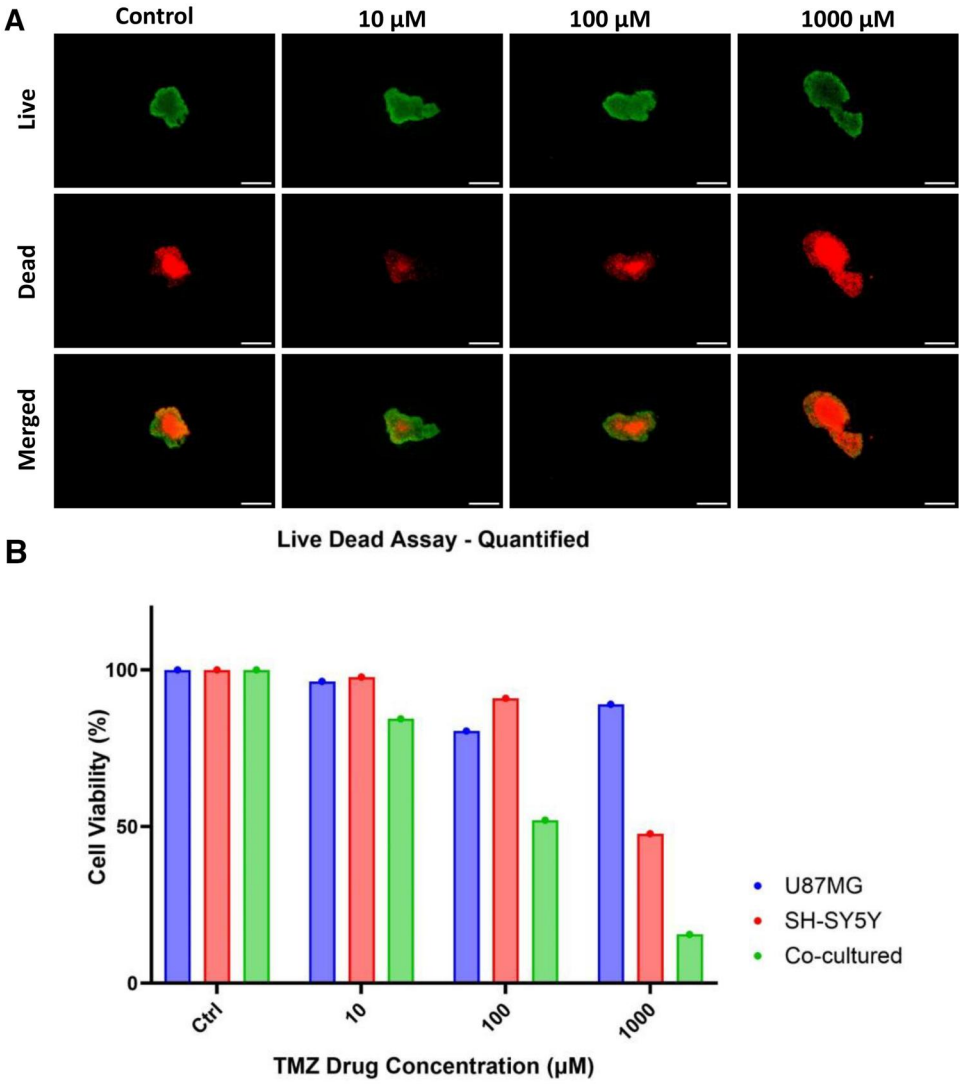

Figure 6. Live/dead assay results: Images from fluorescent microscopy that display both living (green) and dead (red) cells at various TMZ concentrations (Control, 10 μM, 100 μM, and 1000 μM). Live cells are shown in the top row, dead cells are shown in the middle row, and the combined findings are displayed in the bottom row. Dead cell fluorescence increases with increasing TMZ doses, especially at 1000 μM. B) **Live dead assay—quantified**. Cell viability (in percentage) of co-cultured cells (green), U87MG (blue), and SH-SY5Y (red) in response to increasing TMZ concentrations (0 (Ctrl), 10, 100, and 1000 μM) is shown in a bar graph. According to bar graph, all cell lines exhibit high viability at lower concentrations (0 (Ctrl), 10 μM, and 100 μM; however, SH-SY5Y cells show a notable decrease at 1000 μM

Computerised analysis methods, such as biomarker-optimized neural networks, demonstrate superior accuracy in detecting cell death, providing effective tools for assessing treatment responses [38]. These speeds up the creation of tissue-engineered models and increases reproducibility.

In personalized medicine, studies such as Linsley et al. [39] and Carnevali et al. [40] emphasize the utility of patient-derived spheroids in developing personalized medication sensitivity profiles. The analysis conducted using AI improves this process by delivering accurate and quick evaluations, which are essential in reducing rely on animal models while maintaining standards of ethics.

In comparison with conventional human techniques, AI spheroid analysis provides substantial enhancements in accuracy, consistency, and time efficiency. Manual techniques, including visual examination and manual counting, are prone to human error and subjectivity, resulting in diversity in outcomes, particularly when analysing extensive datasets or intricate 3D structures. Conversely, the AI-driven system provides uniform, replicable outcomes, minimizing operator bias and reducing inter-observer variability. The AI-based model exhibited a significant connection with manual cell viability counts, evidenced by a robust R^2 value between predicted and actual data. Moreover, the AI system facilitates the identification of small morphological alterations in spheroids that may be overlooked by manual techniques, so offering a more thorough comprehension of cellular responses to treatments. The automated characteristics of the AI technology significantly enhance time efficiency. The model can analysed hundreds of spheroids in a fraction of the time required for a researcher to manually count cells or evaluate morphological features, providing it extremely ideal for high-throughput applications.

Although it was clear benefits, the AI-driven spheroid analysis system possesses limits that want attention in future work. A main problem is to potential complications with dye penetration during the live/dead experiment. In thick 3D spheroid, the ability of PI and FDA to penetrate consistently can be limited, leading to inaccuracies in viability assessments, particularly in the core of

larger spheroid. Incomplete staining may result in ignoring the proportion of dead cells in the centre of the spheroid. Notably, there are practical ways to alleviate the variability in dye penetration and imaging inconsistencies observed in large spheroids. For instance, for example we have used a one-step multiplexed dye application which can ensure more uniform labelling of spheroids cores and reduce assay variability [31]. Moreover, adopting improved variability dyes with a greater permeability and stability could further minimize inconsistent staining [41]. To address fluorescence signal attenuation with Confocal microscopy, image normalization techniques (such as flat-filed correction) can be employed. In fact, optical clearing treatments can increase spheroid transparency and have been demonstrated to enhance confocal imaging depth by reducing light scattering [42]. Likewise, light-sheet microscopy can offer better imaging depth and minimal phototoxicity, yielding more consistent fluorescence readouts from thick spheroids [43]. Incorporating these solutions would improve the robustness of our viability measurements without requiring new experiments.

A further limitation occurs from the imaging difficulties caused by confocal microscopy, particularly when capturing images of large or dense spheroids. The quality of fluorescence images can be influenced by issues including light scattering, optical aberrations, and depth penetration, especially when imaging deeper areas of the spheroid. Advancements in imaging methods, such light-sheet microscopy and enhanced fluorescent probes, may enhance image quality and address some problems, facilitating more precise study of deeper spheroid regions.

Future advancements in multi-staining techniques may enhance the model's capacity to evaluate both cell viability and functionality simultaneously. Multi-channel imaging, utilizing diverse biomarkers to evaluate multiple facets of cellular health (e.g., proliferation, apoptosis, and necrosis), would yield a more thorough comprehension of spheroid behaviour. This would be especially beneficial in drug screening, where it is crucial to understand not only cell viability but also the unique processes of drug-induced toxicity or therapeutic response.

The implementation of AI-driven spheroid analysis in healthcare environments presents ethical and practical challenges. Maintaining patient data confidentiality and reducing biases in model predictions are essential for balanced results. Compliance with rules like as GDPR and the rigorous assessment of AI models for clinical-grade integrity are crucial. Practically, the capacity for high-throughput workflows, the standardization of imaging and staining methods, and sufficient training for physicians are essential measures for ensuring successful integration into clinical practices. These approaches will facilitate the system's broad acceptance while preserving ethical purity and operational efficiency.

Importantly, the proposed analysis framework is not limited to the cell line used in this study. The deep learning models can be retrained of fine-tuned for spheroids derived from other cancer cell lines, making the model broadly adaptable. In fact, recent deep learning studies on 3D cultures have shown a viability prediction model can generalize well to cell lines and treatment conditions outside of its training data [14]. This suggests that with appropriate learning using a small set of images from new cell type, our segmentation and viability quantification models should perform effectively on different tumour spheroid models. Thus, the model and its methodology could be expanded to other cancer cell lines without fundamental changes to approach.

Conclusion

This study presents an innovative AI-based framework for the analysis of 3D spheroid models, which is significant advancement in cancer research. The two-stage pipeline integrates a U-net model for accurate segmentation of 3D spheroids, achieving a prediction accuracy of 95%, and a CNN Regression Hybrid approach for quantifying live/dead cell percentages, with an R^2value of 98%. This integration of segmentation and viability analysis addresses key challenges in high-throughput evaluations, including environmental variability and morphological characterization. By automating this process, the system enhances scalability, efficiency, and precision, covering the way for its application in drug discovery, toxicity screening, and clinical research.

Adding biomarkers and adopting multimodal AI models can provide deeper insights for complex cell behaviours. Advances in AI techniques, such as self-supervised learning and generative approaches, offer potential to uncover complicated biological patterns. By encouraging cross-disciplinary collaborations, this framework is assured to direct innovations in personalized medicine, therapeutic development, and translational research.

Acknowledgements

Nanasaheb D. Thorat & Ajay K. Mali acknowledges funding under the Research Ireland (Science Foundation Ireland) Irish Research Council (SFI-IRC) pathway program (21/PATH-S/9634). And Department of Physics at the University of Limerick, Ireland. All authors would like to acknowledge their respective departments for the conduct of the study. We sincerely thank Dr Sandeep B. Somvanshi for his valuable feedback and insightful suggestions during the preparation and review of the manuscript.

Author contributions

Ajay K. Mali (Conceptualization [lead], Formal analysis [lead], Investigation [lead], Methodology [lead], Writing—original draft [lead]), Sivasubramanian Murugappan (Formal analysis [supporting], Investigation [supporting], Methodology [supporting], Writing—original draft [supporting]), Jayashree Rajesh Prasad (Methodology [supporting], Writing—review & editing [supporting]), Syed A. M. Tofail (Project administration [supporting], Resources [supporting], Supervision [supporting], Writing—review & editing [supporting]), and Nanasaheb D. Thorat (Conceptualization [lead], Funding acquisition [lead], Project administration [lead], Resources [lead], Supervision [lead], Writing—review & editing [lead])

Supplementary data

Supplementary data are available at *Biology Methods and Protocols* online.

Conflict of interest statement. The authors declare no conflict of interest.

Data availability

The data that support the findings of this study are available from the corresponding author upon request.

References

1. Gheytanchi E, Naseri M, Karimi-Busheri F *et al.* Morphological and molecular characteristics of spheroid formation in HT-29 and Caco-2 colorectal cancer cell lines. *Cancer Cell Int* 2021;**21**: 204–16. no. Dec. https://doi.org/10.1186/S12935-021-01898-9/FIGURES/4
2. Manduca N, Maccafeo E, De Maria R *et al.* 3D cancer models: one step closer to in vitro human studies. *Front Immunol* 2023; **14**:1175503.Apr. https://doi.org/10.3389/FIMMU.2023.1175503/BIBTEX
3. Chen Z, Ma N, Sun X *et al.* Automated evaluation of tumor spheroid behavior in 3D culture using deep learning-based recognition. *Biomaterials* 2021;**272**:120770. https://doi.org/10.1016/J.BIOMATERIALS.2021.120770
4. Shirai K, Kato H, Imai Y *et al.* The importance of scoring recognition fitness in spheroid morphological analysis for robust label-free quality evaluation. *Regen Ther* 2020;**14**:205–14. https://doi.org/10.1016/j.reth.2020.02.004
5. Zhou SK, Greenspan H, Davatzikos C *et al.* A Review of Deep Learning in Medical Imaging: imaging Traits, Technology Trends, Case Studies with Progress Highlights, and Future Promises. *Proc Ieee Inst Electr Electron Eng* 2021;**109**:820–38. https://doi.org/10.1109/JPROC.2021.3054390
6. Weng W, Zhu X. INet: convolutional Networks for Biomedical Image Segmentation. *IEEE Access* 2021;**9**:16591–603. https://doi.org/10.1109/ACCESS.2021.3053408
7. Ö. Çiçek A, Abdulkadir SS, Lienkamp T, Brox *et al.* 3D U-Net: Learning Dense Volumetric Segmentation from Sparse Annotation. Jun. 2016, [Online]. Available: http://arxiv.org/abs/1606.06650
8. Ronneberger O, Fischer P, Brox T. U-net: Convolutional networks for biomedical image segmentation. Lecture Notes in Computer Science (Including Subseries Lecture Notes in Artificial Intelligence and Lecture Notes in Bioinformatics). Vol 9351. Springer Verlag, 2015, 234–41.
9. Esteva A *et al.* Deep learning-enabled medical computer vision. *Nature Research* 2021; https://doi.org/10.1038/s41746-020-00376-2
10. Grexa I, Diosdi A, Harmati M *et al.* SpheroidPicker for Automated 3D Cell Culture Manipulation using Deep Learning. *Sci Rep* 2021; **11**:14813. https://doi.org/10.1038/s41598-021-94217-1
11. Huang G, Liu Z, Van Der Maaten L *et al.* Densely Connected Convolutional Networks. [Online]. Available: https://github.com/liuzhuang13/DenseNet.
12. Liu T, Siegel E, Shen D. Deep Learning and Medical Image Analysis for COVID-19 Diagnosis and Prediction. *Annu Rev Biomed Eng* 2022;**24**:179–201. https://doi.org/10.1146/ANNUREV-BIOENG-110220-012203/CITE/REFWORKS
13. Lacalle D, Castro-Abril HA, Randelovic T *et al.* SpheroidJ: an Open-Source Set of Tools for Spheroid Segmentation. *Comput Methods Programs Biomed* 2021;**200**:105837. https://doi.org/10.1016/J.CMPB.2020.105837
14. Chiang C-C, Anne R, Chawla P *et al.* Deep learning unlocks label-free viability assessment of cancer spheroids in microfluidics. *Lab Chip* 2024;**24**:3169–82. https://doi.org/10.1039/d4lc00197d
15. Leiwe MN, Fujimoto S, Baba T *et al.* Automated neuronal reconstruction with super-multicolour Tetbow labelling and threshold-based clustering of colour hues. *Nat Commun* 2024;**15**: 5279. https://doi.org/10.1038/s41467-024-49455-y
16. Pereira AR, Redzic N, Van Vooren S *et al.* Development, Validation, and Implementation of an Augmented Multiwell, Multitarget Quantitative PCR for the Analysis of Human Papillomavirus Genotyping through Software Automation, Data Science, and Artificial Intelligence. *J Mol Diagn* 2024;**26**:781–91. https://doi.org/10.1016/j.jmoldx.2024.05.012
17. Chieregato M, Frangiamore F, Morassi M *et al.* A hybrid machine learning/deep learning COVID-19 severity predictive model from CT images and clinical data. *Sci Rep* 2022;**12**:4329. https://doi.org/10.1038/s41598-022-07890-1
18. Murugappan S, Mali AK, Tofail SAM *et al.* Astrocyte-neuron co-cultured 3d tumor spheroid model for anti-cancer drug screening. 2024; https://doi.org/10.1101/2024.11.11.622957
19. Shen D, Wu G, Suk H-I. Deep learning in medical image analysis. *Annu Rev Biomed Eng* 2024;**25**:24. https://doi.org/10.1146/annurev-bioeng-071516
20. Murcia-Gómez D, Rojas-Valenzuela I, Valenzuela O. Impact of image preprocessing methods and deep learning models for classifying histopathological breast cancer images. *Applied Sciences (Switzerland* 2022;**12**:11375. https://doi.org/10.3390/app122211375
21. Faryna K, van der Laak J, Litjens G. Automatic data augmentation to improve generalization of deep learning in H&E stained histopathology. *Comput Biol Med* 2024;**170**:108018. https://doi.org/10.1016/j.compbiomed.2024.108018
22. Wang S, Yang DM, Rong R *et al* . Pathology Image Analysis Using Segmentation Deep Learning Algorithms. *Am J Pathol* 2019;**189**: 1686–98. https://doi.org/10.1016/j.ajpath.2019.05.007
23. Gupta D, Kose U, Khanna A et al. Deep Learning for Medical Applications with Unique Data—Google Books. Accessed: Dec. 30, 2024. [Online]. Available: https://books.google.ie/books? hl=en&lr=&id=aZxBEAAAQBAJ&oi=fnd&pg=PP1&dq=Application+of+deep+learning+techniques+for+biomedical+image+segmentation+Gupta,+S.,+et+al.+(2021)&ots=jI8Fgh1n-o&sig=x4nD_-0anzM0QbHv9dUwRZDguMY&redir_esc=y#v=onepage&q&f=false
24. Yang S, Xiao W, Zhang M *et al.* Image data augmentation for deep learning: a survey. Apr. 2022 [Online]. Available: http://arxiv.org/abs/2204.08610
25. Kingma DP, Adam JB. A method for stochastic optimization. Dec. 2014, [Online]. Available: http://arxiv.org/abs/1412.6980
26. Chetty G, Yamin M, White M. A low resource 3D U-Net based deep learning model for medical image analysis. *Int J Inf Tecnol* 2022;**14**: 95–103. https://doi.org/10.1007/s41870-021-00850-4
27. James, G Witten, D Hastie, T *et al.* An introduction to statistical learning. 2023, https://doi.org/10.1007/978-3-031-38747-0
28. Ajala S, Muraleedharan Jalajamony H, Nair M et al. Comparing machine learning and deep learning regression frameworks for accurate prediction of dielectrophoretic force. *Sci Rep* 2022;**12**. https://doi.org/10.1038/s41598-022-16114-5
29. Rueden CT, Schindelin J, Hiner MC *et al.* ImageJ2: imageJ for the next generation of scientific image data. *BMC Bioinformatics* 2017;**18**:529. https://doi.org/10.1186/s12859-017-1934-z
30. Sirenko O, Mitlo T, Hesley J *et al.* High-content assays for characterizing the viability and morphology of 3d cancer spheroid cultures. *Assay Drug Dev Technol* 2015;**13**:402–14. https://doi.org/10.1089/adt.2015.655
31. Ferraro R, Di Franco J, Caserta S *et al.* The morphology of cell spheroids in simple shear flow. *Front Phys* 2024;**12**:1347934. https://doi.org/10.3389/fphy.2024.1347934
32. Taha AA, Hanbury A. Metrics for evaluating 3D medical image segmentation: analysis, selection, and tool. *BMC Med Imaging* 2015;**15**:29. https://doi.org/10.1186/s12880-015-0068-x
33. Milletari F, Navab N, Ahmadi S-A. V-Net: Fully convolutional neural networks for volumetric medical image segmentation. Jun. 2016, [Online]. Available: http://arxiv.org/abs/1606.04797
34. Kuhn M, Johnson K. Applied predictive modeling. *Appl Predic Modeling* 2013;1–600. https://doi.org/10.1007/978-1-4614-6849-3/COVER

35. Willmott CJ, Matsuura K. Advantages of the mean absolute error (MAE) over the root mean square error (RMSE) in assessing average model performance. *Clim Res* 2005;**30**:79–82. https://doi.org/10.3354/CR030079
36. Pinto B, Henriques AC, Silva PMA et al. Three-dimensional spheroids as in vitro preclinical models for cancer research. *Pharmaceutics* 2020;**12**:1–38.
37. Lee RY, Wu Y, Goh D et al. Application of Artificial Intelligence to In Vitro Tumor Modeling and Characterization of the Tumor Microenvironment. *Adv Healthc Mater* 2023;**12**. https://doi.org/10.1002/adhm.202202457
38. Linsley JW, Linsley DA, Lamstein J et al. Superhuman Cell Death Detection with Biomarker-Optimized Neural Networks. *Sci Adv* 2021;**7**:eabf8142.
39. Carnevali F, Forciniti S, Onesto V et al. Advancements in Cancer Research: 3D Models, Single-Cell, and Live-Cell Techniques for Better Insights. *Adv Ther (Weinh)* 2024;**7**:2400351. https://doi.org/10.1002/adtp.202400351
40. Langhans SA. Using 3D in vitro cell culture models in anticancer drug discovery. *Expert Opin Drug Discov* 2021;**16**:841–50. https://doi.org/10.1080/17460441.2021.1912731
41. Ramu V, Wijaya LS, Beztsinna N *et al.* Cell viability imaging in tumor spheroids via DNA binding of a ruthenium (II) light-switch complex. *Chem Commun (Camb)* 2024;**60**:6308–11. https://doi.org/10.1039/d4cc01425a
42. Silva DN, Costa EC, Rodrigues CF *et al.* Influence of cleart and cleart2 agitation conditions in the fluorescence imaging of 3d spheroids. *Int J Mol Sci* 2020;**22**:1–13. https://doi.org/10.3390/ijms22010266
43. Diosdi A, Piccinini F, Boroczky T *et al.* Single-cell light-sheet fluorescence 3D images of tumour-stroma spheroid multicultures. *Sci Data* 2025;**12**:492. https://doi.org/10.1038/s41597-025-04832-0

Biology Methods and Protocols, 2025, 10, 1–10
https://doi.org/10.1093/biomethods/bpaf030
Methods Article